

# Computational Exploration of Multistable Elastic Knots

MICHELE VIDULIS, EPFL, Switzerland  
YINGYING REN, EPFL, Switzerland  
JULIAN PANETTA, UC, Davis, USA  
EITAN GRINSPUN, University of Toronto, Canada  
MARK PAULY, EPFL, Switzerland



Fig. 1. A deployable structure built from a multistable elastic knot. The two center images show different orientations of the same 3D equilibrium state.

We present an algorithmic approach to discover, study, and design multistable elastic knots. Elastic knots are physical realizations of closed curves embedded in 3-space. When endowed with the material thickness and bending resistance of a physical wire, these knots settle into equilibrium states that balance the forces induced by elastic deformation and self-contacts of the wire. In general, elastic knots can have many distinct equilibrium states, i.e. they are *multistable* mechanical systems. We propose a computational pipeline that combines randomized spatial sampling and physics simulation to efficiently find stable equilibrium states of elastic knots. Leveraging results from knot theory, we run our pipeline on thousands of different topological knot types to create an extensive data set of multistable knots. By applying a series of filters to this data, we discover new transformable knots with interesting geometric and physical properties. A further analysis across knot types reveals geometric and topological patterns, yielding constructive principles that generalize beyond the currently tabulated knot types. We show how multistable elastic knots can be used to design novel deployable structures and engaging recreational puzzles. Several physical prototypes at different scales highlight these applications and validate our simulation.

CCS Concepts: • **Computing methodologies** → **Shape modeling; Modeling and simulation.**

Authors' addresses: Michele Vidulis, [michele.vidulis@epfl.ch](mailto:michele.vidulis@epfl.ch), EPFL, Switzerland; Yingying Ren, [yingying.ren@epfl.ch](mailto:yingying.ren@epfl.ch), EPFL, Switzerland; Julian Panetta, [jpanetta@ucdavis.edu](mailto:jpanetta@ucdavis.edu), UC, Davis, USA; Eitan Grinspun, [eitan@cs.toronto.edu](mailto:eitan@cs.toronto.edu), University of Toronto, Canada; Mark Pauly, [mark.pauly@epfl.ch](mailto:mark.pauly@epfl.ch), EPFL, Switzerland.

Permission to make digital or hard copies of all or part of this work for personal or classroom use is granted without fee provided that copies are not made or distributed for profit or commercial advantage and that copies bear this notice and the full citation on the first page. Copyrights for components of this work owned by others than ACM must be honored. Abstracting with credit is permitted. To copy otherwise, or republish, to post on servers or to redistribute to lists, requires prior specific permission and/or a fee. Request permissions from [permissions@acm.org](mailto:permissions@acm.org).

© 2023 Association for Computing Machinery.

XXXX-XXXX/2023/5-ART \$15.00

<https://doi.org/10.1145/nnnnnnn.nnnnnnn>

Additional Key Words and Phrases: elastic knots, multistability, physics-based simulation, numerical optimization, fabrication

## ACM Reference Format:

Michele Vidulis, Yingying Ren, Julian Panetta, Eitan Grinspun, and Mark Pauly. 2023. Computational Exploration of Multistable Elastic Knots. 1, 1 (May 2023), 15 pages. <https://doi.org/10.1145/nnnnnnn.nnnnnnn>

## 1 INTRODUCTION

Knots are a fundamental concept in mathematics and physics. As mathematical objects, knots are mainly studied as topological equivalence classes of embeddings of a circle into 3D space [Adams 2004]. As physical objects, knots can be classified into two main categories: tight knots and loose knots. Tight knots, commonly used in medical sutures, climbing, or boating, leverage friction to block sliding. Their geometric configurations alter the mechanical properties of the rope in which they are tied, such as its tensile strength [Stasiak et al. 1999].

On the other hand, one can tie a knot in a thin elastic rod or wire, and join its ends to form a loose knot (Figure 1). The resulting *elastic knot* will relax into a configuration that minimizes its elastic energy subject to topology-preserving non-interpenetration constraints. Despite the simplicity of the material system, even a single knot can exhibit a surprising variety of geometrically distinct equilibrium shapes. In other words, loose elastic knots are *multistable* (see Figure 2 and Figure 8).

Multistability is a fundamental mechanical principle with widespread applications ranging from simple bottle caps or light switches to energy harvesting [Kim and Kim 2012], medical devices [Roetter et al. 2009], morphing structures [Zhang et al. 2021], and reprogrammable mechanical metamaterials [Chen et al. 2021].

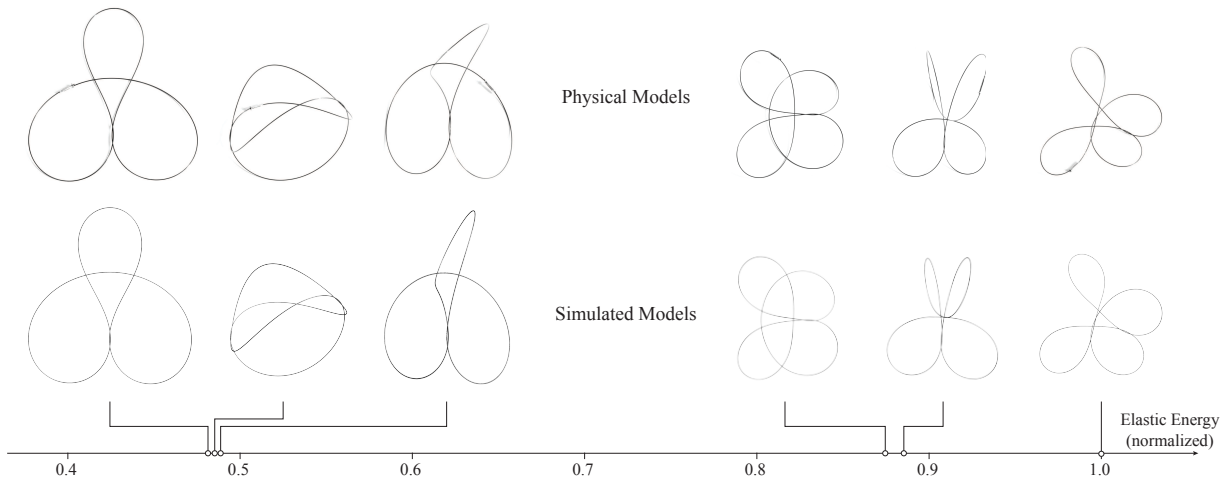


Fig. 2. Even the figure-eight knot ( $4_1$ ), one of the simplest knots with only four crossings, exhibits many geometrically distinct equilibria. To our knowledge, only the three leftmost states with lower elastic energy have been reported in the literature.

Here, we present a study of multistable elastic knots with two or more equilibrium states. These stable knot embeddings can be continuously transformed into each other without changing topology, but are separated by energy barriers. In general, we cannot hope to find such local minima analytically in a complex energy landscape that is defined by the elasticity of the wire and self-contact constraints. Thus, we turn to numerical optimization.

*Contributions.* We present several technical innovations to build a computational pipeline for the discovery and exploration of multistable elastic knots. Specifically, we apply a geometric sampling scheme for topological knots, implement a robust simulation method, and design filters and interactive tools for analyzing the space of elastic knots. We apply our method to

- create and publicly disseminate an extensive data set of multistable knots,
- perform an analysis of this dataset to identify geometrical and topological patterns in the space of elastic knots,
- report previously undocumented stable states of elastic knots, revealing their high degree of multistability, and
- introduce new deployable structures and a new class of recreational puzzles.

We validate our approach with several physical prototypes that consistently exhibit the multistability predicted by the simulation. Code and data for this paper can be found at <https://go.epfl.ch/knots>.

## 2 RELATED WORK

Our computational pipeline for multistable knots is a specific instance of the problem of exploring complex energy landscapes. We briefly discuss related methods in this general domain before reviewing previous research that links more directly to our approach. Specifically, our method builds upon prior work on (i) sampling closed curves, (ii) studying properties of elastic knots in a theoretical framework, and (iii) modeling and simulating physical knots.

*Exploring complex energy landscapes.* Finding multiple local minimizers of a high-dimensional, nonlinear, and non-convex objective function is relevant for a wide range of problems such as protein structure prediction [Liwo et al. 1999], optimal object arrangement [Pintér 2002], and network optimization [Guisewite 1995]. Typically, these local minima are found as byproducts of a *global optimization* algorithm seeking a global minimizer. Global optimization is computationally hard apart from special cases (e.g., convex problems), and a systematic, deterministic search of high-dimensional energy landscapes is thwarted by the curse of dimensionality. Therefore, many global optimization algorithms combine local optimization with random sampling. Existing methods include stochastic tunneling [Wenzel and Hamacher 1999], parallel tempering [Earl and Deem 2005] and genetic algorithms [Zbigniew 1996]. We cannot easily apply the meta-heuristics proposed in these algorithms to our simulation, however, due to the challenging topological constraints. Moreover, we are interested not only in global constrained minimizers of elastic energy (i.e., the equilibria of lowest energy), but also the numerous other stable equilibrium configurations that a knot can assume.

*Sampling closed curves.* As we represent our knots as discrete curves, we aim to sample the finite-dimensional space of closed 3D polygons with  $n$  vertices. Many approaches have been proposed to sample random polygons. Examples include ordered sets of points on the unit sphere  $S^2$  [Even-Zohar 2017], equilateral curves in  $\mathbb{R}^3$  [Cantarella and Shonkwiler 2016], and planar 4-valent bicolored graphs [Liang and Mislow 1994]. Unfortunately, no efficient algorithm is known for determining whether two given closed curves are topologically equivalent [Hass 1998]. This would be needed to identify which equilibrium configurations reached from these randomly sampled curves are stable states of the same elastic knot. To address this issue, several Markov chain algorithms have been proposed to sample curves of fixed knot topology. These methods start from a valid embedding of known knot type, and then iteratively modify

this embedding while preserving its topology [Alvarado et al. 2011]. Efficient implementations of these algorithms exist for polygons on the cubic lattice  $\mathbb{Z}^3$  [Quake 1995; Rensburg and Whittington 1991] and serve as a basis for our work (see Section 5).

*Elastic knots.* The study of physical knots is often based on energy functionals defined on closed 3D curves [Strzelecki and von der Mosel 2017]. Such functionals can capture physical properties of the material with which the knots are tied, such as their electrostatic charge [Fukuhara 1988], self-repulsion [O’Hara 2003], ropelength [Cantarella et al. 2002; Gonzalez and Maddocks 1999], or elastic energy [Bartels and Reiter 2020; Langer and Singer 1984].

A widely studied problem in the context of knot energies is the computation of canonical shapes of knots [Buck and Orloff 1993]. The canonical embedding is identified with the global energy minimizer, subject to topological non-penetration constraints.

Langer and Singer [1985] show how self-contact points are fundamental for the emergence of non-trivial geometries in closed elastic rods. The authors prove that, when considering only bending energy, *a closed knotted wire cannot rest in stable equilibrium without points of self-contact*. Contact-free equilibria have been documented in simple *open* knots tied into paper strips, for certain displacements and rotations of the elastic ribbon’s ends [Moulton et al. 2018].

Elastic knots are often studied by means of energy functionals that model elasticity and self-repulsion. The energy-minimizing configurations have been computed numerically, e.g. by gradient descent [Bartels and Reiter 2021], or even analytically for some specific basic knot types under an assumption of vanishing wire thickness [Diao et al. 2021; Gerlach et al. 2017].

Several works report the existence of multiple stable states for specific simple elastic knots [Avvakumov and Sossinsky 2014; Bartels and Reiter 2021; Gilsbach et al. 2021]; see also Figure 2. Similar conclusions about multi-stability were obtained using models based on purely geometric deformations of polygonal curves [Buck and Rawdon 2004; Gallotti and Pierre-Louis 2007], as well as the more accurate Kirchhoff rod theory [Furrer et al. 2000], which describes the behavior of elastic rods that can bend and twist [Jawed et al. 2018]. Explicit solutions have been derived for intrinsically straight Kirchhoff rods in the absence of self-contact points [Swigon et al. 1998]. In the case of knotted rods with self-contacts, analytical solutions are only known for rings [Coleman and Swigon 2000] and torus knots [Coleman and Swigon 2004]. Multiple configurations satisfying the equations are shown to exist for the same physical rod. The difficulty in generalizing these results to more complex topologies, barring simple cases with regular geometries [Audoly et al. 2007; Clauvelin et al. 2009], is that the location of contact points cannot be assumed a priori.

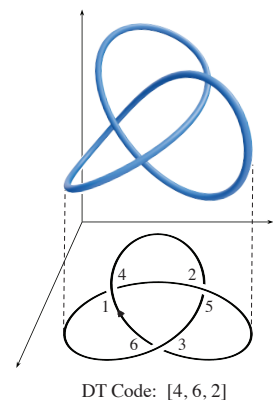
*Knot simulation.* In mechanical engineering, numerical simulations of elastic rods are commonly based on Finite Element discretizations of the smooth equations [Durville 2012; Johanns et al. 2021; Meier et al. 2014]. In computer graphics, alternative models have been proposed, including STRANDS [Pai 2002], Super-Helices [Bertails et al. 2006], and CORDE [Spillmann and Teschner 2007], based on Cosserat’s rod theory [Soler et al. 2018], and Discrete Elastic Rods [Bergou et al. 2010, 2008], which discretizes Kirchhoff’s theory. The key idea of these models is to represent a rod with a

reduced set of variables using a framed curve that separates the encoding of the centerline from the orientation of the cross-section. In particular, CORDE has been used to simulate tight knots [Spillmann and Teschner 2008]. To avoid self-penetrations, contact forces are computed at each time step to recover a collision-free configuration. Alternative solutions involve the discretization of self-repulsive knot energies [Bartels and Reiter 2020, 2021], which, if properly tuned, penalize close-to-singular configurations. Bartels and colleagues developed *KNOTEVOLVE*, a numerical optimization framework to simulate self-repelling confined curves. The software is publicly accessible through a web interface<sup>1</sup>. Despite being very effective for knot untying [Yu et al. 2021], globally-defined repulsive energies are not well suited to model local phenomena such as self-contacts, since interaction forces are non-zero even between points that are distant in space. Moreover, large displacements can potentially lead to missed collisions, causing topology changes in the simulated structure. Some recent works address this challenge by combining collision detection with smooth, local contact energy terms that ramp up as edges penetrate each other [Choi et al. 2021; Li et al. 2020, 2021]. *Continuous-time* collision detection [Wang et al. 2021] can be used in these frameworks to compute admissible, collision-free step sizes to guarantee topology preservation.

*Jumping knots.* In the early 1980s, Langer introduced interesting geometric puzzles based on elastic knots that have been an inspiration for our work [Gardner 1983]. The elastic wires, coined as jumping knots by Langer, automatically deploy into unique 3D equilibrium states when removed from a flat envelope (Figure 11). The goal of these puzzles is then to fit the knot back into the envelope by manually finding the deformation from the 3D state into a multi-covered circle. We use our computational pipeline to discover new jumping knots in the style of Langer. We also generalize the concept of jumping knots and propose new types of knot-based puzzles as discussed in Section 8.

### 3 MATHEMATICAL KNOTS

We first introduce some basic concepts and terminology of mathematical knots relevant to our work. Knot theory is a branch of topology that studies knots as mathematical entities [Adams 2004]. A knot is an embedding of the topological circle  $S^1$  in 3D space. A *knot type* is the equivalence class generated by an ambient isotopy relation, i.e. the set of all closed curves that can be continuously deformed into each other without self-intersections. The *knot diagram* of a closed curve is any 2D projection that is injective away from a finite number of *crossings* where two segments of the projected curve intersect transversely. Knot diagrams encode the topological structure of the curve by indicating which of the two strands passes over the other at each crossing (see inset).



<sup>1</sup><https://aam.uni-freiburg.de/agba/forschung/knotevolve/>

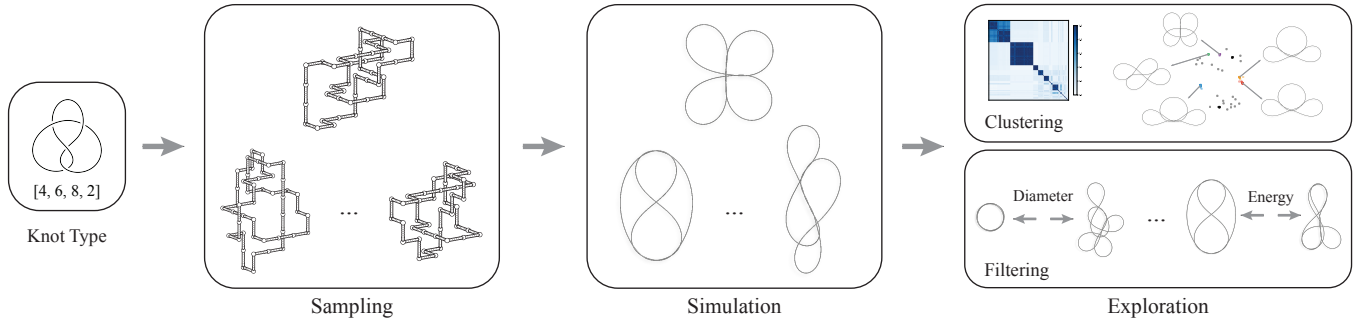


Fig. 3. Overview of our computational pipeline. For a given knot type, we sample random embeddings as initial states for our elastic rod simulation that optimizes the curve geometry towards a local minimum of the elastic energy. Clustering and filtering tools then facilitate analysis and exploration.

**Knot Tables.** Knot types have been classified in tables that contain different ways of encoding their topological structure. These tables commonly provide additional information on symmetry types, chirality, and other numerical or polynomial invariants, i.e. quantities that have the same value for topologically equivalent curves.

The first classification of knots as topological objects is due to Tait [1884]. To sort knots by complexity, Tait used the *crossing number*, i.e. the minimum number of crossings across all possible knot diagrams of a certain knot type. His table enumerated more than one hundred knots with up to ten crossings. We refer to tabulated knots using Alexander–Briggs notation  $x_y$ , where  $x$  denotes the crossing number and  $y$  is an arbitrary index. For example, the figure-eight knot of Figure 2 is denoted by  $4_1$ . A letter ( $a$  or  $n$ ) in the subscript indicates whether a knot is alternating or not [Adams 2004], but this distinction is not relevant for our purposes.

Research to extend Tait’s work is still ongoing. The most recent tabulation considers all knot types with up to nineteen crossings, resulting in more than 350 million topologically distinct knots [Burton 2020]. The *KnotInfo* database [2022] collects a variety of information about all the knot types up to twelve crossings.

**Encoding Knot Types.** The Dowker-Thistlethwaite (DT) notation is a way of encoding a knot type by means of a sequence of integer numbers. Given an oriented knot diagram, the corresponding DT code can be computed by tracing along the knot curve and labeling visited crossings (see inset above). Conversely, from a given DT code we can reconstruct a knot diagram, which can in turn be converted to a 3D curve [Scharein 1998]. A complete definition of the DT notation can be found in Appendix A. We employ DT codes to construct knots in our pipeline as discussed in Section 5.

Among the many possible alternative representations of knot types, we mention closed braids [Alexander 1923], as they have an intuitive geometric interpretation and allow easy generation of multi-covered circle embeddings. We apply the braid representation in the design of knot puzzles as discussed in Section 8.

## 4 OVERVIEW

Our central goal is to discover and explore multistable behavior in elastic knots. For this purpose, we propose a computational pipeline summarized in Figure 3. Given a topological knot type, we first create a 3D embedding of the corresponding centerline curve based

on an input DT code. We then sample new embeddings by applying a series of topology-preserving transformations (Section 5). For each embedded curve, we construct an elastic rod with appropriate physical properties, straight rest shape, and circular cross-section. We then minimize the elastic potential energy of the rod to find an equilibrium state, while preserving the knot topology using contact modeling and continuous collision detection (Section 6). Sampling and simulation provide us with a large set of (not necessarily distinct) equilibrium states for a given knot type. To facilitate analysis and exploration, we introduce a hierarchical clustering scheme to group knot embeddings based on a geometric similarity measure and present a series of filters to extract the most relevant knot embeddings for specific design objectives (Section 7). We run our pipeline on a large class of tabulated knots and perform an analysis of equilibrium states across knot types. To the best of our knowledge, this is the first documented attempt of providing a large-scale overview of the shapes attainable by knotted elastic wire in equilibrium. The results of this analysis as well as several application examples are discussed in Section 8.

## 5 SAMPLING KNOT EMBEDDINGS

Given a knot type, we use its DT code to construct a geometric embedding. We then manipulate this initial curve using a series of random, topology-preserving operations on a cubic lattice to create new embeddings of the same knot type (see Figure 4).

**Sampling a knot on the cubic lattice.** Knot embeddings on the cubic lattice  $\mathbb{Z}^3$  are constrained to have vertices at integer coordinates and edges connecting adjacent grid locations. To sample a knot on the lattice, we first generate a polygonal embedding from the DT code using KnotPlot<sup>2</sup> [Scharein 1998]. The embedding is then refined and rounded onto the lattice. To ensure that rounding does not alter the knot topology, we scale the polygonal curve so that the minimum distance between any two nodes is large enough to prevent rounding two nonadjacent nodes to the same lattice location. We apply 100 iterations of the repulsive curves algorithm [Yu et al. 2021] prior to this scaling to increase the minimum distance and hence reduce the required scaling factor.

<sup>2</sup><https://www.knotplot.com>

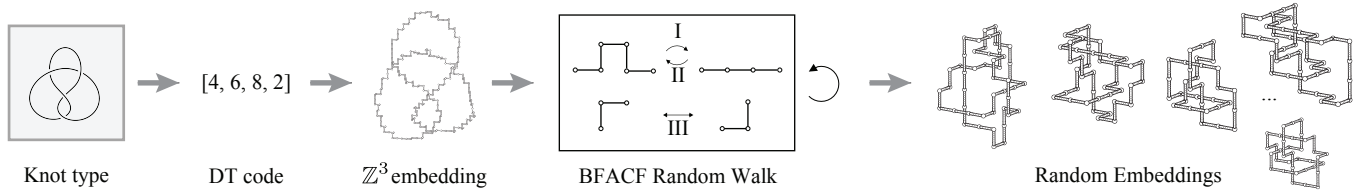


Fig. 4. Sampling random embeddings of a given knot type. The DT code is transformed into an initial polygon which is rounded to integer coordinates with guarantee of topology preservation. On the cubic lattice  $\mathbb{Z}^3$ , the BFACF algorithm performs a random series of local, topology-preserving modifications to the knot geometry that produce a set of distinct embeddings.

*Random self-avoiding walks.* Given a polygon on the cubic lattice, we generate a set of geometrically distinct embeddings of the given knot type by applying random sampling. Specifically, we use the BFACF algorithm traditionally employed in the study of particle physics [Berg and Foerster 1981] and knotted polymers [Quake 1995]. This approach applies three different types of local modifications on the lattice, indicated by the roman numerals I, II, and III as shown in Figure 4. These moves are attempted iteratively by choosing random locations on the curve. Since the curve is sampled on the cubic lattice, it can be easily determined if a move alters the knot topology. A move is applied, and the curve configuration is updated accordingly, only if the knot topology is preserved. An implementation of the BFACF algorithm is available in KnotPlot [Scharein 1998].

The above sampling algorithm has ergodicity classes that correspond to knot types [Rensburg and Whittington 1991]. This means that any two cubic lattice polygons with the same knot type can be transformed into each other using only the moves of BFACF.

Since the computed lattice curves will serve as initialization for the equilibrium simulation described below, we need to ensure an adequate curve resolution. Too few vertices can lead to convergence issues in contact handling due to large kinks in the curves, while too many vertices diminish performance. We empirically found  $n = 400$  vertices to give a sufficiently fine discretization to faithfully model curvature in all knot types with up to 12 crossings. For more complex knots, a higher sampling rate might be necessary.

To reach the desired curve resolution, we introduce bias in the BFACF algorithm by adapting the probabilities of applying type I, II, and III moves. Following [Scharein et al. 2009], we sample moves in two cycles. First, we bias the algorithm towards more of the length-increasing type II moves. We stop when the number of nodes equals  $10n$ . Then, we increase the relative probability of length-decreasing type I moves and continue the random walk until the curve has exactly  $n$  nodes. The probabilities of each of the moves are controlled by a single adjustable parameter as discussed in detail by Madras and Slade [1996].

## 6 SIMULATION

The result of applying our sampling algorithm is a set of random curve embeddings of a given knot type on the cubic lattice. These curves, when interpreted as the centerlines of elastic wires, are far from stable equilibria. We thus propose a simulation method that optimizes each curve towards a local minimum of elastic energy

under non-interpenetration constraints to preserve knot topology. In contrast to prior work [Coleman and Swigon 2000, 2004], we make no assumptions on the number, location, or geometry of contact regions. Moreover we employ contact energy terms that more faithfully model physical collisions compared to the global repulsive interactions typical of classical knot energies [Bartels and Reiter 2021; Rawdon and Simon 2006; Yu et al. 2021].

Our implementation uses the discrete elastic rod model [Bergou et al. 2010, 2008]. The centerline curve of the discrete knotted wire is represented by a closed polyline with  $n$  nodes. In order to represent the orientation of the cross-section at each point along the rod and measure twist, a material frame angle variable  $\theta^j$  is introduced for each edge  $0 \leq j < n$ ; this angle specifies the rotation of the cross-section around the edge tangent (relative to an orthonormal reference frame that is maintained adapted to the edge tangent via parallel transport). The total energy  $E_{\text{rod}}(\mathbf{x}, \boldsymbol{\theta})$  of a discrete elastic rod accounts for bending, twisting, and stretching deformations, where  $\mathbf{x} \in \mathbb{R}^{n \times 3}$  collects the node positions  $\mathbf{x}_i$ , and  $\boldsymbol{\theta} \in \mathbb{R}^{n+1}$  collects the material frame angle variables along with an additional angle  $\Theta$ .

The scalar variable  $\Theta$  represents the twist injected before connecting the two ends. When this variable is left free in the optimization, the rod is allowed to untwist and relax into an equilibrium configuration with zero twisting energy. However, by fixing  $\Theta$  to a prescribed value, we are able to assign the *link* of the (discrete) framed curve, a topological invariant that is preserved during the simulation (see Appendix C for more details). Accounting for link is important when considering deformations of a knot from one state into another. A typical example is our application to knot puzzles discussed in Section 8. More details on our implementation of closed rods are provided in the supplemental material.

*Contact Handling.* Reliably computing stable states of an elastic knot requires robust handling of self-contacts. Specifically, we need to guarantee preservation of the polyline topology during optimization.

We adopt the variational approach proposed by Li and colleagues [2020; 2021], which achieves these goals by introducing a smooth potential energy to model contact forces and employing continuous-time collision detection [Wang et al. 2021]. Equilibrium states can then be found by minimizing a total potential energy defined as the sum of the elastic energy of the wire and a barrier term  $E_{\text{contact}}$  penalizing interpenetrations:

$$\{\mathbf{x}^*, \boldsymbol{\theta}^*\} = \arg \min_{\mathbf{x}, \boldsymbol{\theta}} E_{\text{rod}}(\mathbf{x}, \boldsymbol{\theta}) + \omega E_{\text{contact}}(\mathbf{x}). \quad (1)$$

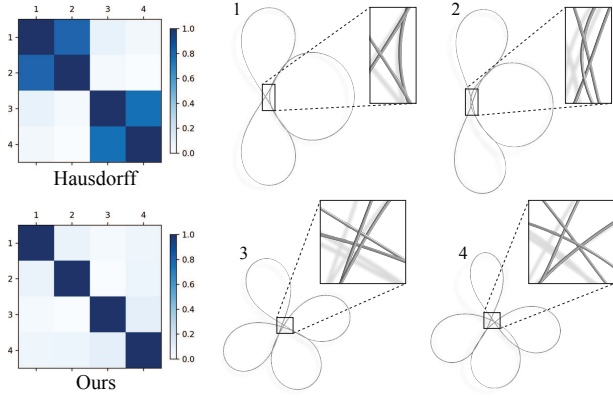


Fig. 5. Pairwise similarity for some equilibria of knot  $6_1$ . The Hausdorff distance shown at the top has difficulties distinguishing between the pairs of states 1-2 and 3-4, which are geometrically close, but have distinctly different contact patterns. Our correlation-based measure more easily separates these embeddings.

The scalar weight  $\omega \in \mathbb{R}$  balances the relative contribution of elastic energy and contact energy. Rather than using the publicly available C-IPC code, which simulates rods with contact but does not model twisting, we opted to combine our full discrete elastic rod implementation described above with the IPC Toolkit [Ferguson et al. 2020]. We refer to prior works ([Bergou et al. 2010, 2008; Li et al. 2020, 2021]) for more details on these energy terms.

*Numerical Solver.* We optimize Equation (1) using a modified Newton solver based on the code from [Panetta et al. 2019]. To account for rigid motions and global twisting of the isotropic cross-section, which if left unconstrained result in a singular total potential energy Hessian  $H = \nabla^2 E_{\text{rod}} + \omega \nabla^2 E_{\text{contact}}$ , we add a tiny multiple of the identity before attempting to compute a Cholesky factorization. By shifting all eigenvalues up by a small amount, this modification essentially eliminates rigid motion from the Newton step and, more importantly, ensures a positive definite matrix in neighborhoods of stable equilibria. This strategy achieved significantly faster convergence than other alternatives we tried using variable pin constraints (both local ones based on constraining the orientation of a single edge and more global ones appropriately fixing displacement components of distant vertices). The shift magnitude is chosen as  $\epsilon \lambda_{\min}$ , where  $\epsilon$  is a user-defined parameter (fixed at  $\epsilon = 10^{-4}$  in our experiments), and  $\lambda_{\min}$  is the minimum nonzero eigenvalue of  $\nabla^2 E_{\text{rod}}$  evaluated on the simulated wire in a straight configuration. If the Cholesky factorization of the shifted Hessian fails, it implies  $H$  was indefinite (rather than positive semidefinite) and a further shift is applied to the spectrum to make it positive definite.

We note that the sparsity pattern of  $\nabla^2 E_{\text{contact}}$  changes whenever the contact constraint set changes (while the sparsity pattern of  $\nabla^2 E_{\text{rod}}$  is fixed); for best performance, we detect these changes and recompute the symbolic factorization only in this case. Our threshold for convergence is based on the gradient norm and a requirement that  $H$  be positive semidefinite (to rule out unstable equilibria).

## 7 EXPLORATION

Launching our simulation from hundreds of randomly sampled embeddings (see Section 7.4) yields a large number of numerical solutions to the equilibrium problem. To facilitate interactive exploration of the dataset, it is helpful to group geometrically similar embeddings—for instance, those corresponding to the same physical equilibrium state. We note that even when the numerical solutions do approximate the same equilibrium, they deviate from each other for several reasons: (1) the physical equilibrium is not unique, as any global rotation or cyclic reparametrization of one equilibrium centerline produces another; (2) the minimization problem is solved only to a finite level of accuracy, meaning each numerical solution lies in a neighborhood of states also satisfying the convergence criterion; and (3) the energy landscape of our discrete model can contain spurious nearby local minima that for certain applications should be considered to be in the same equivalence class. We therefore propose an interactively tunable clustering method to achieve this grouping. By adjusting a single sensitivity parameter, the user can browse through a hierarchical arrangement of equilibrium states to visually identify the most relevant embeddings. These embeddings can additionally be sorted and filtered according to different geometric or physical attributes.

### 7.1 Similarity measure

Our clustering involves making pairwise comparisons between any two equilibrium centerlines of a given knot type. In our exploration pipeline, this comparison must be performed millions of times, making direct measures of geometric similarity between two space curves, such as Hausdorff or Fréchet distances, computationally prohibitive [Alt and Godau 1995]. We instead compute the similarity of two knot embeddings from differential signatures based on curvature  $\kappa$  and torsion  $\tau$  of the centerline curves.

For our polygonal curves, we define discrete curvature  $\kappa_i$  as the turning angle between the edges meeting at node  $i$  divided by the Voronoi area of that node (the average incident edge length). We define discrete torsion  $\tau^j$  as the angle between the binormal vectors of the endpoint nodes of edge  $j$  divided by the length of that edge. Binormals are computed from the cross product of the two incident edge vectors [Carroll et al. 2014]. From this definition, it is apparent that discrete torsion becomes numerically unstable as curvature approaches zero, i.e. when consecutive edge vectors align. Indeed, the torsion of a continuous curve can blow up in the neighborhood of inflection points [Hord 1972]. This is problematic since inflection points are common in our knots (see Figure 8) and the resulting extreme, mesh-dependent peaks in the discrete torsion function will dominate the similarity metric. We address this issue by multiplying the torsion profile with the corresponding curvature value (which vanishes at the problematic points) to eliminate the singularity and obtain a well-behaved torsion measure. In other words, we consider the two profiles  $K = [\kappa_1, \dots, \kappa_n]$  and  $T = [\kappa_1 \bar{\tau}_1, \dots, \kappa_n \bar{\tau}_n]$ , where  $\bar{\tau}_i = \frac{1}{2}(\tau^{i-1} + \tau^i)$  is the averaged torsion of the two edges adjacent to node  $i$ .

Our similarity measure is based on the discrete cross-correlation of the profiles  $(K_1, T_1)$  and  $(K_2, T_2)$  of two knot embeddings. Specifically, for two discrete curvature signature vectors  $K_1, K_2 \in \mathbb{R}^n$ , we

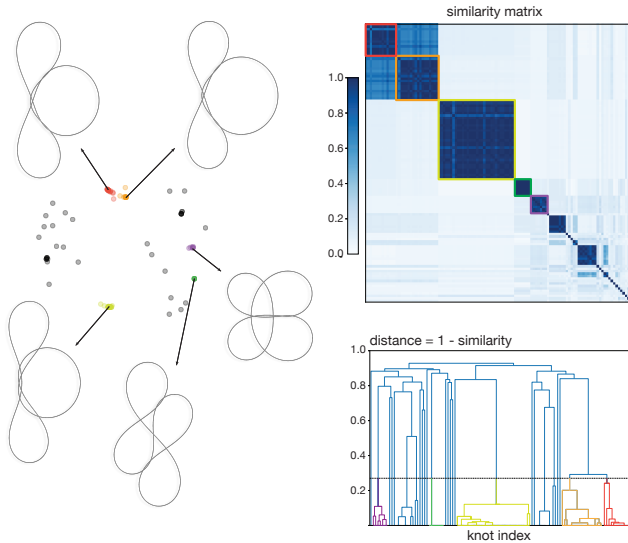


Fig. 6. Hierarchical clustering for knot  $7_7$ . Equilibrium states are progressively merged according to the pairwise similarities shown in the matrix plot. The scatter plot on the left has been created from the similarity matrix via multi-dimensional scaling. Depending on the user-selected threshold, geometrically distinct, but similar embeddings can be grouped into the same equivalence class. For example, the currently separated red and orange clusters will merge into one cluster as the distance threshold is increased.

compute a normalized discrete cross-correlation

$$(K_1 \star K_2)[s] := \frac{K_1 \cdot \text{roll}(K_2, s)}{\|K_1\| \|K_2\|},$$

where  $\text{roll}(K_2, s)[i] := K_2[(i + s) \bmod n]$  cyclically permutes a vector. We then calculate a normalized curvature-torsion cross-correlation  $T_1 \star T_2$  analogously and compute the normalized similarity measure as  $\max_s [(K_1 \star K_2)[s]]_+ + [(T_1 \star T_2)[s]]_+ \in [0, 1]$ , where  $[\cdot]_+ := \max(\cdot, 0)$  clamps negative values to zero (to prevent the signs of two negative correlations from canceling). We efficiently evaluate the cross-correlation using a discrete Fast Fourier Transform [Proakis and Manolakis 2006].

As illustrated in Figure 5, our similarity measure can distinguish between geometrically close embeddings that have different self-contact patterns. This is important, for example, in the design of knot puzzles as discussed in Section 8.3.

*Symmetries.* Our similarity metric is designed to be invariant under rigid motions and cyclic reparametrizations. When desired, we can in addition account for reflective symmetry and reversal of curve orientation, which define states of equal potential energy. Whether these states are topologically equivalent to the originals depends on the knot type. Some knots are known to be chiral: an oriented curve with chiral knot type is not ambient-isotopic to its mirror image, nor to a copy with reversed orientation [Kodama and Sakuma 1992]. Orientation reversal can be accounted for in our similarity measure by also computing *convolutions* of the curve signatures in addition to correlations. Mirroring corresponds to

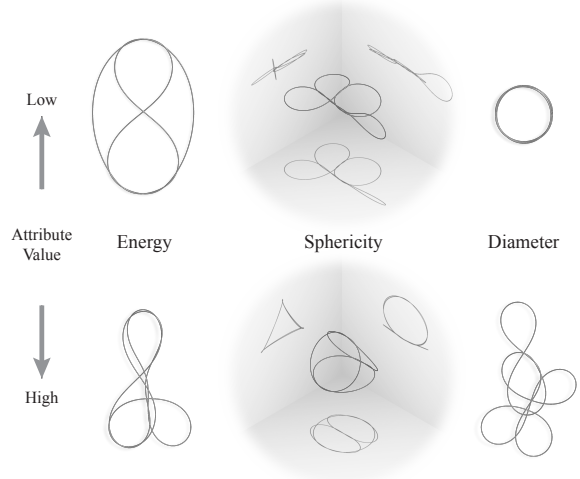


Fig. 7. Filtering sorts embeddings according to different physical and geometric attributes. Total elastic *energy* (left) increases with the square of curvature. *Sphericity* (center) measures closeness to a sphere, here illustrated with three orthogonal shadow projections to better convey the 3D shape. *Diameter* (right) measures the maximum distance between any two points in the curve. The two embeddings in each column have the same topology. From left to right the knot types are  $9_5$ ,  $9_{35}$ , and  $11_{a,57}$ .

inverting the sign of torsion. We then take the maximum of all these measures to define the final similarity score.

## 7.2 Hierarchical Clustering

Clustering supports interactive exploration by grouping geometrically similar equilibrium states to reduce visual complexity. We use agglomerative (i.e. bottom-up) hierarchical clustering. Given the pairwise similarities of all polygonal knot embeddings, we compute a tree diagram by iteratively merging data points and clusters that are most similar. To measure the distance between two clusters in the process, we use the *complete linkage* method, which takes the maximum distance between elements in the two groups, and tends to result in compact clusters [Everitt et al. 2011]. The distance values for each merge are recorded. These values can then be used to support interactive exploration by manually selecting a cutting threshold as illustrated in Figure 6. For low values of the threshold, different datapoints form clusters on their own. As the threshold is increased, geometrically similar states merge, facilitating the identification of recurrent geometries.

The same hierarchical clustering technique is used to adaptively estimate the number of initial embeddings to sample for each knot type, as explained in Section 8.

## 7.3 Filtering

We have observed that elastic knots exhibit a surprisingly large number of equilibrium states with diverse properties (Figure 8). To support analysis, we propose a series of filters that allow sorting equilibrium states according to different physical and geometric quantities. These filters facilitate the discovery of knots with specific properties, such as the deployable structures and knot puzzles we

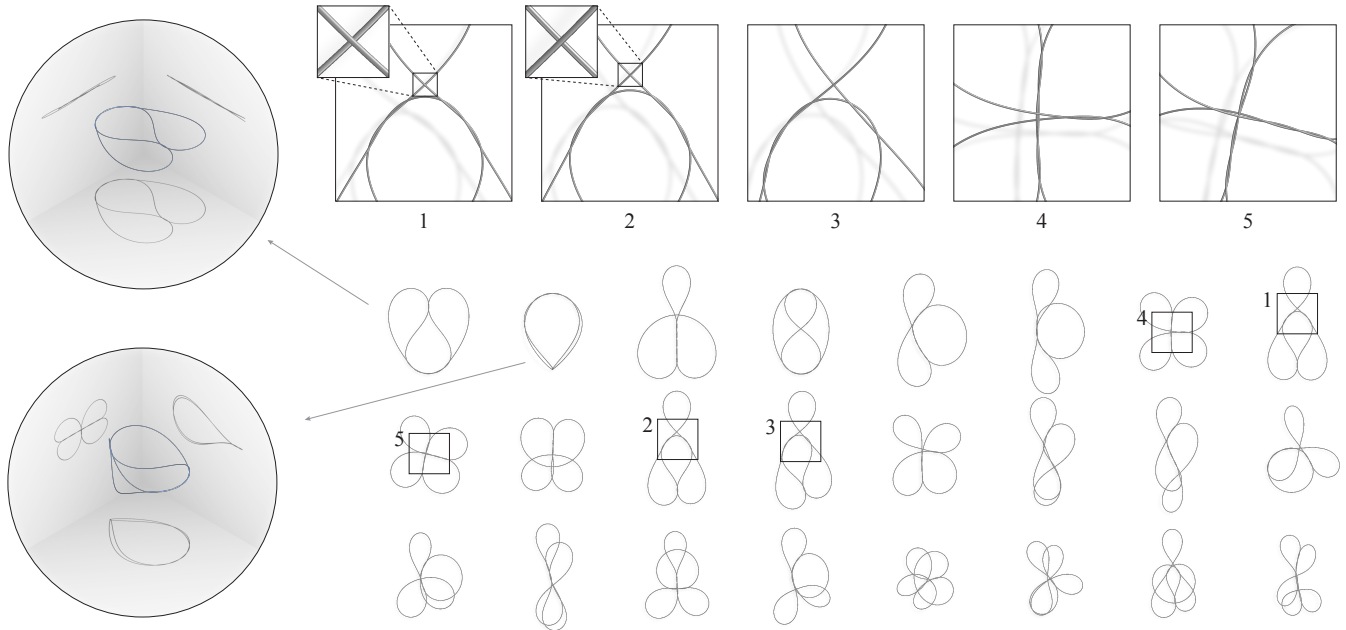


Fig. 8. Elastic knots show a great variety of equilibrium shapes. We show a subset of the equilibria of the knot  $8_1$  sorted by increasing elastic energy from left to right and top to bottom. While some of these states appear geometrically identical, our similarity measure can distinguish differences in contact pattern as illustrated in the zooms. Only one of these equilibria has a distinctly 3D shape (bottom left).

present in Section 8. Below we list filters that we have applied in our exploration so far. Additional filters can be designed and incorporated into our analysis framework as needed for specific applications.

*Physical Attributes.*

- *Energy* quantifies the elastic energy  $E_{rod}$ , giving some indication of how difficult it is to deform the knot into this equilibrium state.
- *Stiffness* is measured as the smallest positive eigenvalue of the full simulation energy Hessian  $H$ .
- *Maximum Stress* induced by bending assesses the potential for material failure. It is computed for a rod with Young’s modulus  $E$  and circular cross-section radius  $r$  as  $\sigma_{max} = rE \max_i \|(\kappa\mathbf{b})_i\|$ , where  $(\kappa\mathbf{b})_i$  is the discrete curvature binormal of the discrete elastic rods model [Bergou et al. 2008] evaluated at node  $i$ .

*Geometric Attributes.*

- *Curvature* indicates the total curvature of the centerline  $\int |\kappa| ds$ , measured as  $\sum_i \kappa_i$  for our polygonal curves.
- *3D-ness* is defined as the aspect ratio of the oriented bounding box of the knot centerline (the shortest box edge length divided by the longest).
- *Sphericity* measures the distance to a sphere as the standard deviation of the distance of node positions  $\mathbf{x}_i$  from the knot centroid.
- *Diameter* is defined as the maximum distance between any two points on the curve.

Figure 7 illustrates some of these filters, which can be applied in any combination. For example, to extract equilibria that are close to multi-covered circles, we first sort according to high sphericity and then according to low 3D-ness. As we discuss in detail in Section 8, we can also apply filters across different knot types to extract knots with specific characteristics from our data set.

7.4 Dataset of Elastic Knot Equilibrium States

We ran our pipeline on all the knots available from the KnotInfo knot table [Livingston and Moore 2022] to build a data set of elastic knots for all 2,977 knot types with up to 12 crossings. We also sampled more complex knot types, but did not yet perform a comprehensive computation of the latest knot table that contains more than 350 million knot types [Burton 2020] and would thus require trillions of sampling computations and billions of simulations.

The boundary conditions imposed at this stage allow the ends of the rod to rotate, resulting in twist-free equilibrium configurations. This enables the framed curves we sample in this exploratory phase to be fully recovered from the centerline polygon alone. If desired, the value of the link can be computed using Călugăreanu’s relation  $Lk = Tw + Wr$  [Călugăreanu 1961], where twist  $Tw = 0$ , and writhe  $Wr$  depends on the centerline but not on the framing. See Appendix C for more details on how these quantities are computed.

In our pipeline, sampling initial embeddings has a negligible computational cost. Rather, the cost is dominated by the simulation phase, with balanced cost contributions from solving for the Newton descent direction and line search backtracking to a feasible collision-free step. This motivates our use of adaptive sampling to selectively reduce the costs of simulation.

In particular, we first compute 50 initial states for each knot type and simulate their relaxation. We continue to progressively sample more cubic lattice embeddings in batches of 10. Every sampling cycle, we evaluate the information contained in the batch by computing an importance score  $S$ . The definition of  $S$  is based on the geometric similarity of the new equilibria with all the previously computed configurations, weighted by the energy of the new states. The score takes values in  $[0, 1]$ , where 1 indicates strong evidence that an additional sampling cycle could generate yet unknown equilibria with relatively low elastic energy. Sampling only continues if  $S > 0.1$ . We stop sampling when a maximum bound of 500 samples is reached. Please refer to our supplemental material for more details on how the score is computed, and an evaluation of the robustness of these sampling heuristics.

All the simulations were performed on a Linux workstation with a 64-Core AMD Ryzen Threadripper 3990X Processor and 128GB of RAM using 14.8h of total compute time. We simulated the equilibrium states for 416,980 random cubic lattice samples, across all the 2,977 knot types up to 12 crossings. The adaptive sampling generated a median value of 90 samples per knot type. For 95% of knot types, our sampling criterion truncated the sampling process. The remaining 5% of knot types, for which the sampling process was stopped at 500 samples, remain candidates for further exploration. Overall, adaptive sampling provided a 70% reduction in compute time compared to sampling 500 states for all knot types.

The full data set as well as the source code of our implementation can be found at <https://go.epfl.ch/knots>.

## 8 RESULTS

Figure 8 gives an indication of the geometric richness of the equilibrium states of knotted wires. Since the geometry of these knots is best appreciated in a 3D viewer, we encourage the reader to explore our supplemental material, where 3D models of our computed knot equilibria can be found.

We have built physical prototypes from aluminum poles of 8.5mm diameter (Figure 1) and superelastic nitinol wire of 1mm diameter (Figures 2, 12, 14). As illustrated in Figures 2 and 12, our physical prototypes match the simulated predictions well.

### 8.1 Limitations

Before presenting our analysis and application examples, we comment on some limitations of our approach.

Most fundamentally, our randomized sampling approach cannot guarantee an exhaustive search of equilibrium states for a given knot type. Moreover, we have no systematic way of deciding whether nearby solutions of the discrete minimization of Equation (1) as obtained by our *numerical* (hence approximate) method, correspond to a *single* local energy minimizer of the smooth, inequality-constrained formulation; samples of a *level set* that locally minimizes the energy; or samples of distinct equilibrium states separated by small energy barriers. As a consequence, we cannot make precise statements about the number of distinct equilibrium states of any given knot type. In fact, for our simulation model, this number might be infinite for vanishing wire thickness if no upper bound on the elastic energy is imposed.

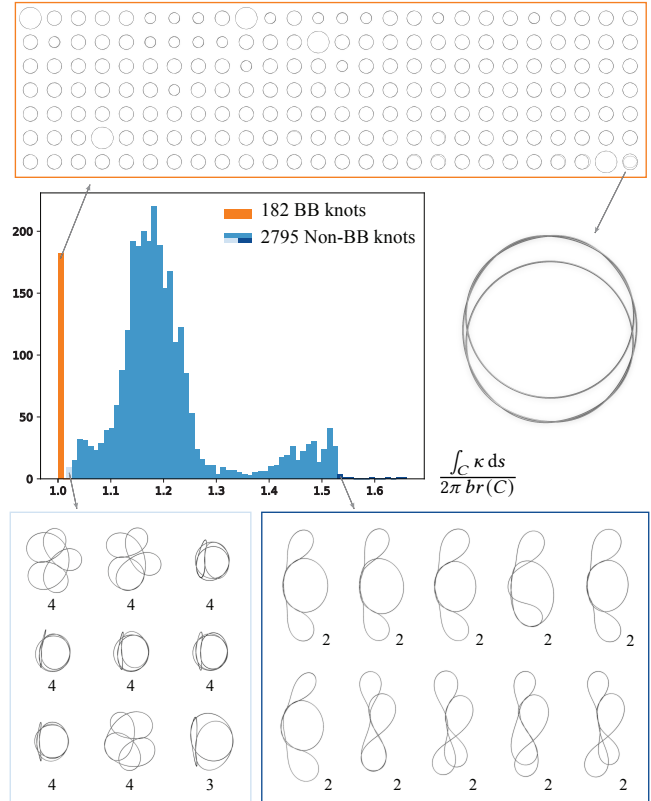


Fig. 9. Curvature analysis. The histogram accumulates for each knot type the equilibrium state with smallest total curvature normalized by Milnor’s minimal bound. Knots with bridge index equal to braid index (BB knots) assume Milnor’s bound in multi-covered circle embeddings (orange). The zoom shows one outlier in the histogram that has a slightly higher total curvature. For this specific knot topology and our chosen wire length to diameter ratio, no ‘flat’ multi-covered circle exists in our data set. The next set of knots close to Milnor’s bound is shown in light blue. At the other end of the spectrum are 2-bridge knots that do not exhibit any embedding close to Milnor’s bound (dark blue). Numbers show the bridge index  $br(C)$ .

In our current data set, the ratio of wire length to wire diameter is fixed at 1,000. While we found that the geometry of equilibrium states does not change drastically with small changes of this ratio, some equilibrium states can disappear as the ratio decreases.

We currently do not model friction at the self-contact regions. This simplification misses some forces acting on the wire, but avoids reporting potentially unstable equilibria that only occur because of friction. In that sense, our method is conservative and only reports states that are stable even without additional friction forces.

### 8.2 Analysis

In general, we observe that loose elastic knots exhibit numerous geometrically distinct equilibrium states (see Figures 2 and 8). While many of these states have high elastic energy and might not be

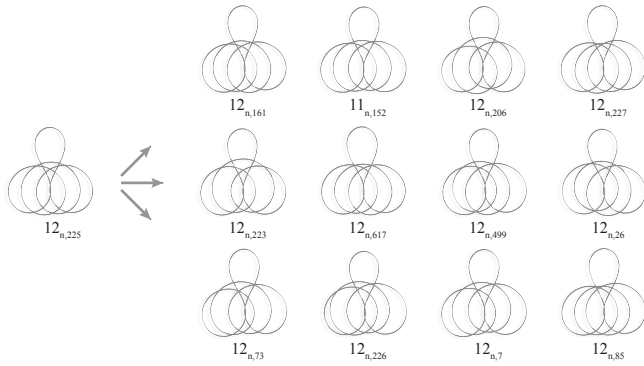


Fig. 10. Cross-topology analysis. For the query knot shown on the left, we extract other knot types with geometrically similar embeddings from our data set.

relevant for most practical applications, this wealth of stable equilibria offers fascinating possibilities to create complex multistable structures with as simple a process as knotting a wire.

To our surprise, we found that for all knots we studied in detail, a significant majority of the observed elastic equilibria are approximately planar. This seems counterintuitive: Since the elastic energy is largely dominated by bending, it might appear natural that the wire would assume a 3D state to reduce the overall curvature. To better understand the behavior of elastic knots, we take a closer look at the curvature of our equilibrium states.

*Milnor’s bound.* Milnor proved one of the fundamental results for geometric knots that relates the total curvature of the embedding to the topology of the knot [Milnor 1950]. For any embedded closed curve  $C$ , Milnor showed that the total curvature is bounded from below. More precisely,  $\int_C \kappa(s) ds > 2\pi br(C)$ , where  $\kappa(s)$  measures curvature and  $br(C)$  is the bridge index of  $C$ , a topological invariant defined in Appendix B. Blair et al. [2020] tabulated  $br(C)$  for knots with up to 14 crossings.

In Figure 9, we compare for each knot type the smallest total curvature of its equilibrium centerlines against the lower bound provided by Milnor’s theorem. Our analysis shows that this bound is (approximately<sup>3</sup>) reached only for multi-covered circle embeddings of knots that have a bridge index equal to their braid index (BB knots, see Appendix B for detailed definitions) as predicted in [Diao et al. 2021]. We note that the lowest-curvature embeddings of *all* BB knots appear in our data set, which provides some evidence that our sampling is effective at recovering at least the low-energy equilibria of each knot type.

For the remaining knots, we observe that knots close to the minimal-curvature bound exhibit geometric commonalities in a few distinct shapes. 3D knots appear as intertwined arrangements of three circles (see also Figure 15). All other knots in this set are approximately planar and feature pretzel-like sub-components. These geometric features lead to low overall curvature as the large arcs compensate for the high curvature of the smaller arcs.

<sup>3</sup>We set a small threshold when filtering with respect to curvature to account for wire thickness. The true bound is only reached in the limit of vanishing wire thickness.

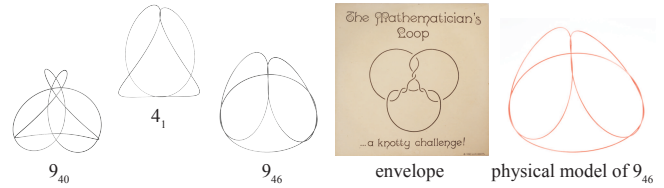


Fig. 11. Langer proposed three different jumping knots that self-deploy from planar, multi-covered circle states. The goal of the puzzle is to fit the 3D state knots back into the envelope.

On the other hand, the knot types with large distance to Milnor’s bound also share interesting geometric features, particularly the occurrence of several tight loops. Topologically, these are all knots with two bridges, where a bridge is a subarc of a knot diagram that contains only over-crossings [Adams 2004]. The existence of tight loops is consistent with a phenomenon known as *braid localization* [Gallotti and Pierre-Louis 2007].

*Cross-topology analysis.* Figure 8 illustrates how we can apply clustering and filtering to study the geometric embeddings of different equilibrium states of the same knot type. Conversely, our analysis tools also allow discovering patterns across different knot topologies. In Figure 10 we select a specific knot embedding and search the database for similar geometries. To reduce the search complexity, we first filter according to geometric attributes. Among this pre-filtered set, we find the most similar embeddings using ICP alignment [Rusinkiewicz and Levoy 2001]. Such a set of knots exhibit geometrically similar stable states but have different topology and different self-contact patterns, and consequently, different mechanical behavior. A potential application could be metamaterial design. A “knitted” network of these knots could be tuned for a specific mechanical behavior by optimizing the distribution of different knot types across the network pattern.

### 8.3 Elastic Knot Puzzles

In this section, we show how our knot exploration algorithms can be used to design knot puzzles. The challenge in these puzzles is to manually deform a given equilibrium state into a different stable (or unstable) state.

*Jumping Knots.* For the special case of Langer’s jumping knots shown in Figure 11, the goal is “to return this exuberant creature to its flat package, by collapsing it into a circular coil.”<sup>4</sup> Using our exploration framework, we have created new Langer-style puzzles shown in Figure 12. Please also see the accompanying video to better appreciate the jumping dynamics.

To find such jumping knots, we first use our filtering method to discover knot types with interesting 3D states. Next we need to determine if the knot “jumps,” i.e. can deploy automatically to such a 3D equilibrium from a planar, unstable multi-covered-circle state. For this purpose, we make use of the braid representation for knots [Adams 2004]. Braids represent a set of intertwined strands and are closely related to knots. In particular, a fundamental result in

<sup>4</sup>Quoted from the original packaging of Langer’s knots.

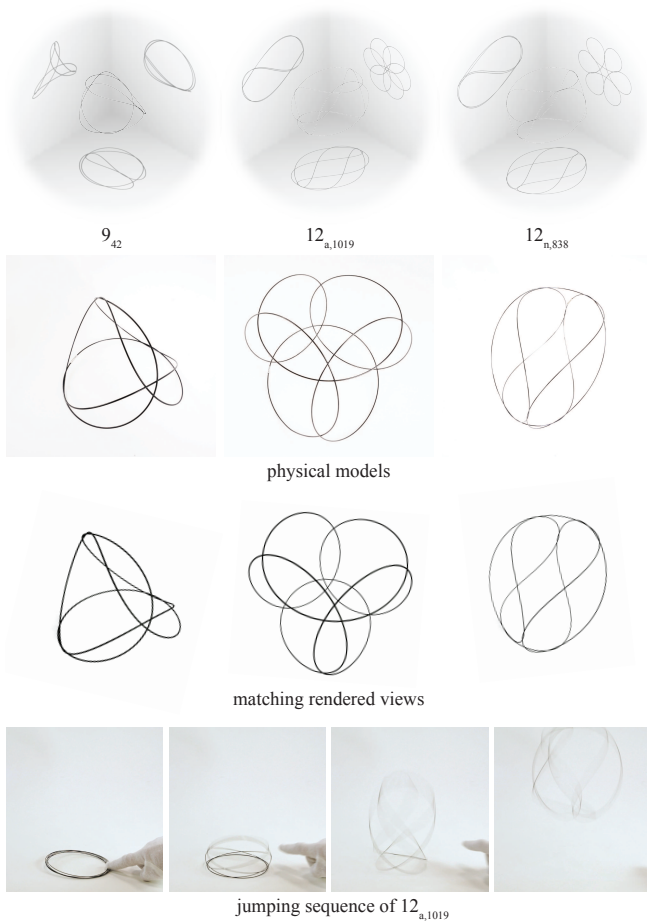


Fig. 12. Our new jumping knots. Top row: Knots with three orthogonal shadow views to give a sense of their 3D equilibrium shapes. Middle rows: Physical models and corresponding views of the simulated embeddings. Bottom row: The multi-covered circle state stores significant potential energy that is released when the knot jumps to assume its 3D equilibrium state.

knot theory states that *every knot can be represented as a closed braid* [Alexander 1923]. A  $k$ -strands braid can be compactly encoded in a *braid word* of arbitrary length containing  $2(k - 1)$  distinct symbols. Braid representations of knot types up to 12 crossings have been computed [Gittings 2004].

Given the braid representation of a knot type, we compute an initial embedding that approximates a multi-covered circle as illustrated in Figure 13 (see also [Scharein 1998]). We then apply our simulation algorithm while imposing a planarity constraint that keeps the knot curve sandwiched between two proximate parallel planes. In this way, the curve relaxes into a minimal-energy multi-covered-circle state. We check that this state is not in equilibrium after releasing the planarity constraint, running our simulation to predict whether the knot deploys towards the 3D target state. However, since our simulation neither accounts for dynamics nor friction, we have to validate this prediction with physical models.



braid word:  $[-1, 2, -3, 4, -1, 2, -3, -1, 2, 4, -3, 4]$

Fig. 13. The braid word encodes the over/under relation of the crossings of braided strands that can be closed along a cylindrical embedding to form a knot. Here we show a multi-covered circle initialization for the knot  $12_{a,1019}$ , one of our new jumping knots.

One subtlety in the design of transformable knots is that we need to ensure that the states we are interested in have the same link. This is required since the physical connection of the two wire ends does not allow the knot to untwist during deformation. We use the Călugăreanu-White-Fuller theorem that states that link ( $Lk$ ) is equal to the sum of twist ( $Tw$ ) and writhe ( $Wr$ ) for a closed smooth curve [Călugăreanu 1961]. To compute the writhe of our discrete polygonal embeddings, we employ the method of [Klenin and Langowski 2000]. In our simulation, we first measure the writhe of the desired 3D state  $Wr_{target}$ , and then set the twist of the initial braid  $B$  so that  $Lk_B = Tw_B + Wr_B = Wr_{target}$ . This computational exploration uncovered many more jumping knots than Langer's originals. Figure 12 shows only a few representatives that we have fabricated to confirm the jumping behavior. To our knowledge, these have not been documented before.

*General Knot Puzzles.* We can generalize Langer's puzzles to knots with multiple stable states. The goal is then to find the deformation between any two or more of these states. Figure 14 shows two of our puzzle designs. In general, we found the manual transformation of multistable knots engaging and satisfying. Our computational pipeline allows designing a multitude of such puzzles, but their effectiveness as a puzzle and difficulty level would need to be evaluated more systematically in a user study.

Since the physical connection blocks twisting, we restrict the search of candidate states to knots with the same writhe (twist is always zero for the knots of our dataset) to ensure that a deformation path exists between any two simulated states of a knot. The physical prototypes are then built in one of the flat configurations that match the chosen value of the writhe. The eventual excess twist is released by letting one of the ends of the wire rotate freely before connecting it to the opposite one. This procedure allows to match the link of the physical and simulated puzzles.

#### 8.4 Generalization

Visual inspection of similar knots can reveal constructive principles that can potentially be generalized. Specifically, we aim to create geometrically similar stable knots that exceed the complexity of existing knot tables.

In Figure 15, we observe that the embeddings retrieved from our database are all composed of three circular parts that are linked through a variable number of crossings at their touching regions. We can easily adapt the number of these crossings separately at each

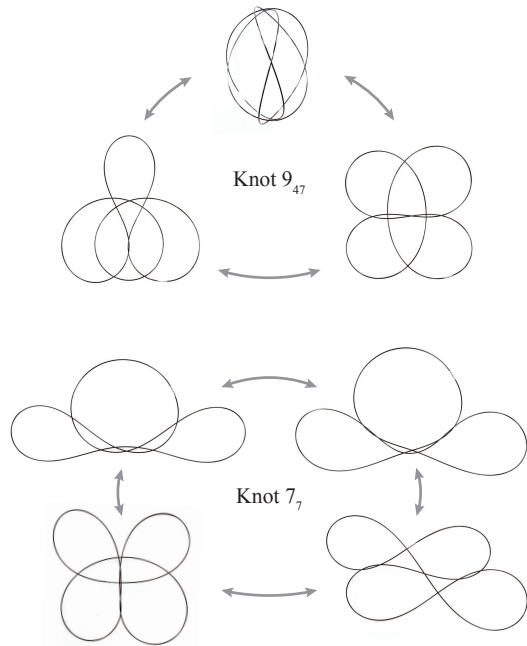


Fig. 14. Physical knot puzzles designed with our approach. Finding the deformation that transforms one equilibrium state to another is not trivial. Top: A relatively easy puzzle with one 3D state. Bottom: A difficult puzzle with two geometrically close, but structurally distinct embeddings (compare with the simulated equilibrium states in Figure 6). The two puzzles’ link values are -3 and 1, respectively.

of the three touching regions through direct edits, and then run our simulation to validate that these newly constructed knots indeed settle into a geometrically similar equilibrium. These new knots exceed 12 crossings and therefore were not present in our database of equilibrium shapes. We do not currently have an effective tool to determine their precise crossing number nor their knot type. In fact, these knots might not yet be classified in any existing table.

*Periodic braids.* When analyzing two of the simplest 3D knots,  $4_1$  and  $9_{40}$ , we observed that their braid representations are periodic. This property can be generalized as shown in Figure 16, again extending beyond the knots in our database. Interestingly, the observed topological pattern also manifests itself in geometric symmetry of the knots’ equilibrium states. The bottom row of Figure 16 shows a view along the main symmetry axis. We observe how the crossing patterns form two regular  $p$ -gons, one at the top and one at the bottom of each embedding. For odd  $p$ , these  $p$ -gons align, while for even  $p$  they are rotated relative to each other by an angle of  $\pi/p$ . We initialized our simulation for these knots from multi-covered circle embeddings obtained from the generalized braid word representations, as illustrated in Figure 13.

Kozlov [2013] proposed a similar procedural approach to generate cyclic knots that he coined NODUS structures. While the specific knot types he presents differ from the ones in Figure 16, it is conceivable that both classes of knots can be defined by some unified symmetry-based generative procedure.

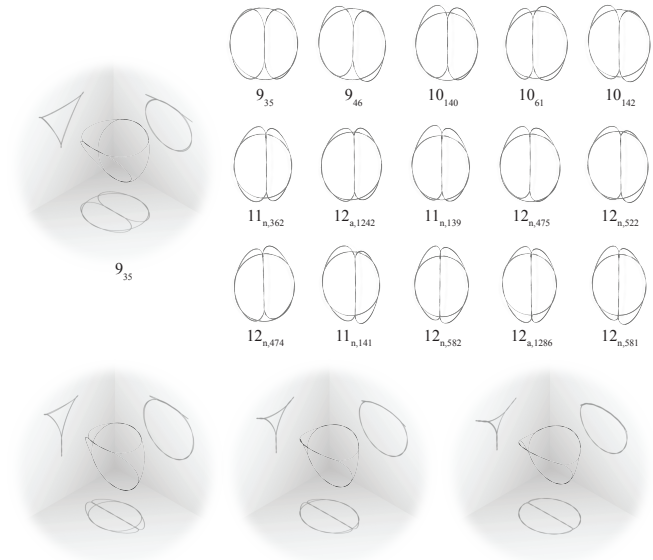


Fig. 15. Constructive generalization. The knots in the top right are retrieved from our database by searching for embeddings close to the 3D state of knot  $9_{35}$  that is composed of three intertwined circles. Generalizing this pattern allows us to design knots with similar geometry that go beyond the 12-crossing knots currently in our data set (bottom row).

### 8.5 Future Work

We have shown some examples of how our interactive knot exploration framework facilitates analysis, generalization, and design of multistable elastic knots. However, we believe that we have only scratched the surface. We expect that other topological and geometric patterns can still be mined from our data set, and that additional computations or extensions to our method can yield richer data sets in the future.

For example, our data set was computed for an elastic wire with a straight rest shape, constant circular cross-section and uniform material properties. These geometric and material parameters affect not only a knot’s equilibrium shape, but also its mechanical behavior. Varying these parameters is supported by our framework and could offer more flexibility for design at the expense of additional computation and data analysis. A quantitative analysis of the deformation of elastic knots under load also will be interesting future work.

Our simulation algorithm allows discovering distinct knot equilibria, but we currently do not have the means to find the transition between such states, nor quantify the energy barrier separating them. A promising avenue for future work is designing computational methods for finding minimum energy paths in configuration space between any two stable states [Vaucher and Reiher 2018], which could help answer many interesting questions related to multistable knots and deployable structures in general.

We can easily extend our simulation algorithm to handle links, i.e. intertwined combinations of several knots. How to effectively design or explore such networks offers numerous avenues for future research. Finally, it would be interesting to combine knotted elastic rods with other deformable elements. For example, multistable

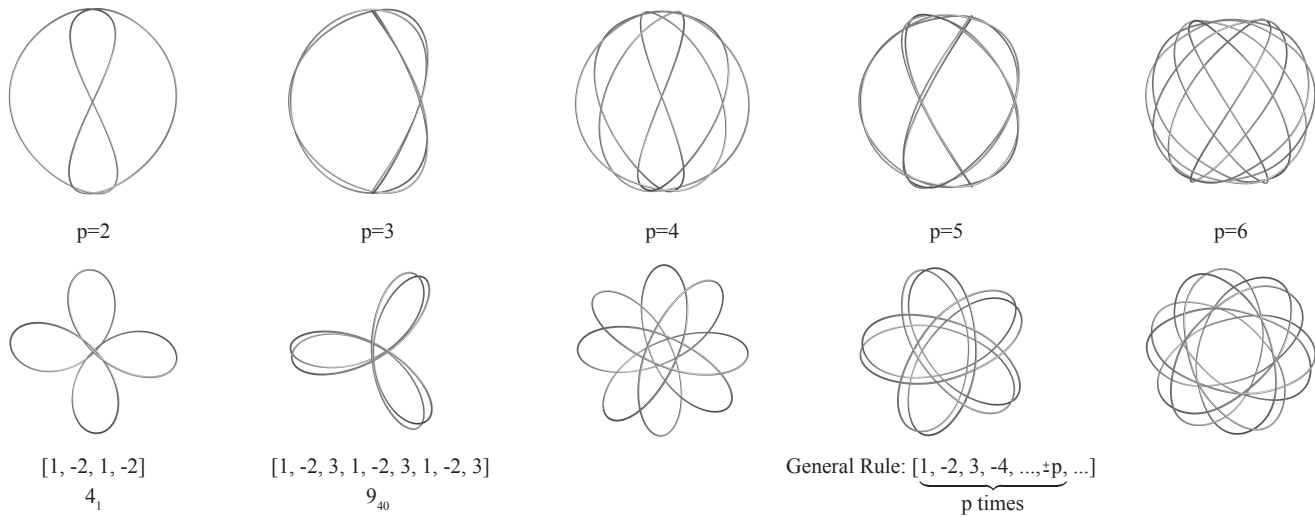


Fig. 16. The knots  $4_1$  (first column) and  $9_{40}$  (second column) have periodic braid words that can be generalized towards more complex knot types outside our knot data set. For each level of periodicity  $p$ , the top and bottom rows show two different views of the same 3D embedding, which has been computed from a multi-covered circle initialization. All knots have the same wire thickness. The length of each wire is set proportional to  $p$ .

elastic knots coupled with fabrics offer new design opportunities for deployable structures such as self-erecting tents.

### 9 CONCLUSION

We presented a computational pipeline for discovering and studying multistable elastic knots. Our analysis offers new insights into the rich space of elastic knots, reveals a surprising abundance of multistable states that have not been documented before, and facilitates the design of new deployable structures and recreational puzzles.

Our algorithms offer versatile tools for the study of elastic knots as well as more complex compound systems of interlinked knots. This opens up a wide space for future exploration and provides many opportunities for the design of advanced transformable structures or metamaterials with unique mechanical properties. Public dissemination of our data set and source code will help facilitate these future explorations.

### ACKNOWLEDGMENTS

We are grateful to Robert Scharein for having developed *KnotPlot* and for his support. We thank John H. Maddocks for helpful comments in the early stages of the projects. We are grateful to Uday Kusupati for his help in building a large-scale prototype and for appearing in the teaser image, and to Filip Goč and Florin Isvoranu who helped fabricating all the physical models. We also thank the reviewers for their valuable feedback. This research was supported by the Swiss National Science Foundation (Grant FNS 514543 / CF 1156) and by a Natural Sciences and Engineering Research Council of Canada (NSERC) Discovery Grant [RGPIN-2021-03733].

### REFERENCES

Colin C. Adams. 2004. *The Knot Book: An Elementary Introduction to the Mathematical Theory of Knots*. American Mathematical Soc.  
 James W. Alexander. 1923. A Lemma on Systems of Knotted Curves. *Proceedings of the National Academy of Sciences of the United States of America* 9, 3 (1923), 93–95.

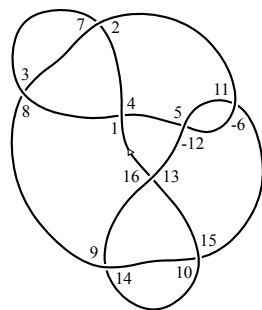
Helmut Alt and Michael Godau. 1995. Computing the Fréchet Distance between Two Polygonal Curves. *Int. J. Comput. Geometry Appl.* 5 (1995), 75–91. <https://doi.org/10.1142/S0218195995000064>  
 Sotero Alvarado, Jorge Alberto Calvo, and Kenneth C. Millett. 2011. The Generation of Random Equilateral Polygons. *Journal of Statistical Physics* 143, 1 (2011), 102–138. <https://doi.org/10.1007/s10955-011-0164-4>  
 Basile Audoly, Nicolas Clavelin, and Sébastien Neukirch. 2007. Elastic Knots. *Physical review letters* 99 (2007), 164301. <https://doi.org/10.1103/PhysRevLett.99.164301>  
 Sergey Avvakumov and Alexey Sossinsky. 2014. On the Normal Form of Knots. *Russian Journal of Mathematical Physics* 21 (2014), 421–429. <https://doi.org/10.1134/S1061920814040013>  
 Sören Bartels and Philipp Reiter. 2020. Numerical solution of a bending-torsion model for elastic rods. *Numer. Math.* 146, 4 (2020), 661–697. <https://doi.org/10.1007/s00211-020-01156-6>  
 Sören Bartels and Philipp Reiter. 2021. Stability of a simple scheme for the approximation of elastic knots and self-avoiding inextensible curves. *Math. Comp.* 90, 330 (2021), 1499–1526. <https://doi.org/10.1090/mcom/3633>  
 B. Berg and D. Foerster. 1981. Random paths and random surfaces on a digital computer. *Phys. Lett. B* 106, 4 (1981), 323–326. [https://doi.org/10.1016/0370-2693\(81\)90545-1](https://doi.org/10.1016/0370-2693(81)90545-1)  
 Miklós Bergou, Basile Audoly, Etienne Vouga, Max Wardetzky, and Eitan Grinspun. 2010. Discrete Viscous Threads. *ACM Trans. Graph.* 29, 4 (2010), 1–10. <https://doi.org/10.1145/1778765.1778853>  
 Miklós Bergou, Max Wardetzky, Stephen Robinson, Basile Audoly, and Eitan Grinspun. 2008. Discrete Elastic Rods. *ACM Trans. Graph.* 27, 3 (2008), 1–12. <https://doi.org/10.1145/1360612.1360662>  
 Florence Bertails, Basile Audoly, Marie-Paule Cani, Bernard Querleux, Frédéric Leroy, and Jean-Luc Lévêque. 2006. Super-Helices for Predicting the Dynamics of Natural Hair. *ACM Trans. Graph.* 25, 3 (2006), 1180–1187. <https://doi.org/10.1145/1141911.1142012>  
 Ryan Blair, Alexandra Kjachukova, Roman Velazquez, and Paul Villanueva. 2020. Wirtinger systems of generators of knot groups. *Communications in Analysis and Geometry* 28, 2 (2020), 243–262. <https://doi.org/10.4310/CAG.2020.v28.n2.a2>  
 Gregory Buck and Jeremy Orloff. 1993. Computing canonical conformations for knots. *Topology and its Applications* 51, 3 (1993), 247–253. [https://doi.org/10.1016/0166-8641\(93\)90079-5](https://doi.org/10.1016/0166-8641(93)90079-5)  
 Gregory Buck and Eric J. Rawdon. 2004. Role of flexibility in entanglement. *Physical Review E* 70, 1 (2004), 011803. <https://doi.org/10.1103/PhysRevE.70.011803>  
 Benjamin A. Burton. 2020. The Next 350 Million Knots. In *36th International Symposium on Computational Geometry (SoCG 2020)*, Vol. 164. 25:1–25:17. <https://doi.org/10.4230/LIPIcs.SoCG.2020.25>  
 Jason Cantarella, Robert B. Kusner, and John M. Sullivan. 2002. On the minimum ropelength of knots and links. *Inventiones mathematicae* 150, 2 (2002), 257–286. <https://doi.org/10.1007/s00222-002-0234-y>  
 Jason Cantarella and Clayton Shonkwiler. 2016. The symplectic geometry of closed equilateral random walks in 3-space. *The Annals of Applied Probability* 26, 1 (2016),

- 549 – 596. <https://doi.org/10.1214/15-AAP1100>
- Daniel Carroll, Eleanor Hankins, Emek Kose, and Ivan Sterling. 2014. A Survey of the Differential Geometry of Discrete Curves. *The Mathematical Intelligencer* 36, 4 (2014), 28–35. <https://doi.org/10.1007/s00283-014-9472-2>
- Tian Chen, Mark Pauly, and Pedro M. Reis. 2021. A reprogrammable mechanical metamaterial with stable memory. *Nature* 589, 7842 (2021), 386–390. <https://doi.org/10.1038/s41586-020-03123-5>
- Andrew Choi, Dezhong Tong, Mohammad K. Jawed, and Jungsoek Joo. 2021. Implicit Contact Model for Discrete Elastic Rods in Knot Tying. *Journal of Applied Mechanics* 88, 5 (2021), 051010. <https://doi.org/10.1115/1.4050238>
- Nicolas Clauvelin, Basile Audoly, and Sébastien Neukirch. 2009. Matched asymptotic expansions for twisted elastic knots: a self-contact problem with non-trivial contact topology. *Journal of the Mechanics and Physics of Solids* 57, 9 (2009), 1623–1656. <https://doi.org/10.1016/j.jmps.2009.05.004>
- Bernard Coleman and David Swigon. 2000. Theory of Supercoiled Elastic Rings with Self-Contact and Its Application to DNA Plasmids. *Journal of Elasticity* 60 (2000), 173–221. <https://doi.org/10.1023/A:1010911113919>
- Bernard Coleman and David Swigon. 2004. Theory of self-contact in Kirchhoff rods with applications to supercoiling of knotted and unknotted DNA plasmids. *Philosophical transactions. Series A, Mathematical, physical, and engineering sciences* 362 (2004), 1281–99. <https://doi.org/10.1098/rsta.2004.1393>
- G. Călugăreanu. 1961. Sur les classes d'isotopie des noeuds tridimensionnels et leurs invariants. *Czechoslovak Mathematical Journal* 11 (1961), 588–625. <https://doi.org/10.21136/CMJ.1961.100486>
- Yuanan Diao, Claus Ernst, and Philipp Reiter. 2021. Knots with Equal Bridge Index and Braid Index. *Journal of Knot Theory and Its Ramifications* (2021). <https://doi.org/10.1142/s0218216521500759>
- Damien Durville. 2012. Contact-friction modeling within elastic beam assemblies: an application to knot tightening. *Computational Mechanics* 49, 6 (2012), 687–707. <https://doi.org/10.1007/s00466-012-0683-0>
- David J. Earl and Michael W. Deem. 2005. Parallel tempering: Theory, applications, and new perspectives. *Physical Chemistry Chemical Physics* 7, 23 (2005), 3910–3916.
- Chaim Even-Zohar. 2017. Models of random knots. *Journal of Applied and Computational Topology* 1, 2 (2017), 263–296. <https://doi.org/10.1007/s41468-017-0007-8>
- Brian S. Everitt, Sabine Landau, Morven Leese, and Daniel Stahl. 2011. *Cluster Analysis* (1 ed.). Wiley. <https://doi.org/10.1002/9780470977811>
- Zachary Ferguson et al. 2020. *IPC Toolkit*. <https://ipc-sim.github.io/ipc-toolkit/>
- Shinji Fukuhara. 1988. Energy of a Knot. In *A Fête of Topology*. Elsevier, 443–451. <https://doi.org/10.1016/B978-0-12-480440-1.50025-3>
- Patrick B. Furrer, Robert S. Manning, and John H. Maddocks. 2000. DNA Rings with Multiple Energy Minima. *Biophysical Journal* 79, 1 (2000), 116–136. [https://doi.org/10.1016/S0006-3495\(00\)76277-1](https://doi.org/10.1016/S0006-3495(00)76277-1)
- R. Gallotti and O. Pierre-Louis. 2007. Stiff knots. *Physical Review E* 75, 3 (2007), 031801. <https://doi.org/10.1103/PhysRevE.75.031801>
- Martin Gardner. 1983. Mathematical Games. *Scientific American* 249, 3 (1983), 18–E8.
- Henryk Gerlach, Philipp Reiter, and Heiko von der Mosel. 2017. The elastic trefoil is the twice covered circle. *Archive for Rational Mechanics and Analysis* 225, 1 (2017), 89–139. <https://doi.org/10.1007/s00205-017-1100-9>
- Alexandra Gilsbach, Philipp Reiter, and Heiko von der Mosel. 2021. Symmetric elastic knots. *Math. Ann.* 385 (2021), 811–844. <https://doi.org/10.1007/s00208-021-02346-9>
- Thomas A. Gittings. 2004. Minimum Braids: A Complete Invariant of Knots and Links. (2004). <https://doi.org/10.48550/arXiv.math/0401051>
- Oscar Gonzalez and John H. Maddocks. 1999. Global curvature, thickness, and the ideal shapes of knots. *Proceedings of the National Academy of Sciences* 96, 9 (1999), 4769–4773. <https://doi.org/10.1073/pnas.96.9.4769>
- G. M. Guisewite. 1995. *Network Problems*. Springer US, Boston, MA, 609–648. [https://doi.org/10.1007/978-1-4615-2025-2\\_11](https://doi.org/10.1007/978-1-4615-2025-2_11)
- Joel Hass. 1998. Algorithms for recognizing knots and 3-manifolds. *Chaos, Solitons & Fractals* 9, 4-5 (1998), 569–581. [https://doi.org/10.1016/S0960-0779\(97\)00109-4](https://doi.org/10.1016/S0960-0779(97)00109-4)
- Richard A. Hord. 1972. Torsion at an inflection point of a space curve. *The American Mathematical Monthly* 79, 4 (1972), 371–374.
- M. Khalid Jawed, Alyssa Novelia, and Oliver M. O'Reilly. 2018. *A Primer on the Kinematics of Discrete Elastic Rods*. Springer International Publishing, Cham. <https://doi.org/10.1007/978-3-319-76965-3>
- Paul Johanns, Paul Grandgeorge, Changyeob Baek, Tomohiko G. Sano, John H. Maddocks, and Pedro M. Reis. 2021. The shapes of physical trefoil knots. *Extreme Mechanics Letters* 43 (2021), 101172. <https://doi.org/10.1016/j.eml.2021.101172>
- Gi-Woo Kim and Jaehwan Kim. 2012. Compliant bistable mechanism for low frequency vibration energy harvester inspired by auditory hair bundle structures. *Smart Materials and Structures* 22, 1 (2012). <https://doi.org/10.1088/0964-1726/22/1/014005>
- Konstantin Klenin and Jörg Langowski. 2000. Computation of writhe in modeling of supercoiled DNA. *Biopolymers* 54, 5 (2000), 307–317.
- K. Kodama and M. Sakuma. 1992. Symmetry groups of prime knots up to 10 crossings. In *Knot 90, Proceedings of the International Conference on Knot Theory and Related Topics*. <https://doi.org/10.1515/9783110875911.323>
- Dmitri Kozlov. 2013. Structures of Periodical Knots and Links as Geometric Models of Complex Surfaces for Designing. *Nexus Network Journal* 15, 2 (2013), 241–255. <https://doi.org/10.1007/s00004-013-0154-8>
- Joel Langer and David A. Singer. 1984. Knotted Elastic Curves in R<sup>3</sup>. *Journal of the London Mathematical Society s2-30*, 3 (1984), 512–520. <https://doi.org/10.1112/jlms/s2-30.3.512>
- Joel Langer and David A. Singer. 1985. Curve straightening and a minimax argument for closed elastic curves. *Topology* 24, 1 (1985), 75–88. [https://doi.org/10.1016/0040-9383\(85\)90046-1](https://doi.org/10.1016/0040-9383(85)90046-1)
- Minchen Li, Zachary Ferguson, Teseo Schneider, Timothy Langlois, Denis Zorin, Daniele Panozzo, Chenfanfu Jiang, and Danny M. Kaufman. 2020. Incremental potential contact: intersection-and inversion-free, large-deformation dynamics. *ACM Trans. Graph.* 39, 4 (2020), 1–20. <https://doi.org/10.1145/3386569.3392425>
- Minchen Li, Danny M. Kaufman, and Chenfanfu Jiang. 2021. Codimensional incremental potential contact. *ACM Trans. Graph.* 40, 4 (2021), 1–24. <https://doi.org/10.1145/3450626.3459767>
- Chengzi Liang and Kurt Mislow. 1994. On amphicheiral knots. *Journal of Mathematical Chemistry* 15, 1 (1994), 1–34. <https://doi.org/10.1007/BF01277546>
- C. Livingston and A. H. Moore. 2022. *KnotInfo: Table of Knot Invariants*. <https://knotinfo.math.indiana.edu/index.php>
- Adam Liwo, Jooyoung Lee, Daniel R Ripoll, Jaroslaw Pillardy, and Harold A Scheraga. 1999. Protein structure prediction by global optimization of a potential energy function. *Proceedings of the National Academy of Sciences* 96, 10 (1999), 5482–5485.
- Neal Madras and Gordon Slade. 1996. *The Self-Avoiding Walk*. Birkhäuser Boston, Boston, MA. <https://doi.org/10.1007/978-1-4612-4132-4>
- Christoph Meier, Alexander Popp, and Wolfgang A. Wall. 2014. An objective 3D large deformation finite element formulation for geometrically exact curved Kirchhoff rods. *Computer Methods in Applied Mechanics and Engineering* 278 (2014), 445–478. <https://doi.org/10.1016/j.cma.2014.05.017>
- J. W. Milnor. 1950. On the Total Curvature of Knots. *The Annals of Mathematics* 52, 2 (1950), 248. <https://doi.org/10.2307/1969467>
- Derek E. Moulton, Paul Grandgeorge, and Sébastien Neukirch. 2018. Stable elastic knots with no self-contact. *Journal of the Mechanics and Physics of Solids* 116 (2018), 33–53. <https://doi.org/10.1016/j.jmps.2018.03.019>
- Jun O'Hara. 2003. *Energy of knots and conformal geometry*. Series on knots and everything, Vol. 33. World Scientific Pub. <https://doi.org/10.1142/5229>
- Oliver M. O'Reilly. 2017. *Modeling Nonlinear Problems in the Mechanics of Strings and Rods*. Springer International Publishing. <https://doi.org/10.1007/978-3-319-50598-5>
- Dinesh K. Pai. 2002. STRANDS: Interactive Simulation of Thin Solids using Cosserat Models. *Computer Graphics Forum* 21, 3 (2002), 347–352. <https://doi.org/10.1111/1467-8659.00594>
- Julian Panetta, Mina Konaković-Luković, Florin Ivoranu, Etienne Bouleau, and Mark Pauly. 2019. X-Shells: a new class of deployable beam structures. *ACM Trans. Graph.* 38, 4 (2019), 1–15. <https://doi.org/10.1145/3306346.3323040>
- János D. Pintér. 2002. *Global Optimization: Software, Test Problems, and Applications*. Springer US, Boston, MA, 515–569. [https://doi.org/10.1007/978-1-4757-5362-2\\_15](https://doi.org/10.1007/978-1-4757-5362-2_15)
- John G. Proakis and Dimitris K Manolakis. 2006. *Digital Signal Processing* (4 ed.). Prentice Hall.
- Stephen R. Quake. 1995. Fast Monte Carlo algorithms for knotted polymers. *Physical Review E* 52, 1 (1995), 1176–1180. <https://doi.org/10.1103/PhysRevE.52.1176>
- Eric J. Rawdon and Jonathan K. Simon. 2006. Polygonal Approximation and Energy of Smooth Knots. *Journal of Knot Theory and Its Ramifications* 15, 04 (2006), 429–451. <https://doi.org/10.1142/S0218216506004543>
- E. J. Janse van Rensburg and S. G. Whittington. 1991. The BFACF algorithm and knotted polygons. *Journal of Physics A: Mathematical and General* 24, 23 (1991), 5553–5567. <https://doi.org/10.1088/0305-4470/24/23/021>
- Adam Roetter, Craig Lusk, and Rajiv Dubey. 2009. Bistable Compliant Extension Aid for a Polycentric Prosthetic Knee (*International Design Engineering Technical Conferences and Computers and Information in Engineering Conference, Vol. 7: 33rd Mechanisms and Robotics Conference*). 241–248. <https://doi.org/10.1115/DETC2009-86990>
- Szymon Rusinkiewicz and Marc Levoy. 2001. Efficient Variants of the ICP Algorithm. In *Proceedings of the Third Intl. Conf. on 3D Digital Imaging and Modeling*, 145–152. <https://doi.org/10.1109/IM.2001.924423>
- R Scharein, K Ishihara, J Arsuaga, Y Diao, K Shimokawa, and M Vazquez. 2009. Bounds for the minimum step number of knots in the simple cubic lattice. *Journal of Physics A: Mathematical and Theoretical* 42, 47 (2009). <https://doi.org/10.1088/1751-8113/42/47/475006>
- Robert G. Scharein. 1998. *Interactive Topological Drawing*. Ph.D. Dissertation. Department of Computer Science, The University of British Columbia.
- Carlota Soler, Tobias Martin, and Olga Sorkine-Hornung. 2018. Cosserat Rods with Projective Dynamics. *Computer Graphics Forum* 37, 8 (2018), 137–147. <https://doi.org/10.1111/cgf.13519>
- Jonas Spillmann and Matthias Teschner. 2007. CORDE: Cosserat Rod Elements for the Dynamic Simulation of One-Dimensional Elastic Objects. In *Eurographics/SIGGRAPH Symposium on Computer Animation*. <https://doi.org/10.2312/SCA/SCA07/063-072>

- Jonas Spillmann and Matthias Teschner. 2008. An Adaptive Contact Model for the Robust Simulation of Knots. *Computer Graphics Forum* 27, 2 (2008), 497–506. <https://doi.org/10.1111/j.1467-8659.2008.01147.x>
- Andrzej Stasiak, Akos Dobay, Jacques Dubochet, and Giovanni Dietler. 1999. Knotted Fishing Line, Covalent Bonds, and Breaking Points. *Science* 286, 5437 (1999). <https://doi.org/10.1126/science.286.5437.11a>
- Paweł Strzelecki and Heiko von der Mosel. 2017. Geometric curvature energies: facts, trends, and open problems. In *New Directions in Geometric and Applied Knot Theory*, 8–35. <https://doi.org/10.1515/9783110571493-002>
- David Swigon, Bernard D. Coleman, and Irwin Tobias. 1998. The elastic rod model for DNA and its application to the tertiary structure of DNA minicircles in mononucleosomes. *Biophysical Journal* 74, 5 (1998), 2515–2530. [https://doi.org/10.1016/S0006-3495\(98\)77960-3](https://doi.org/10.1016/S0006-3495(98)77960-3)
- Peter Guthrie Tait. 1884. On Knots, Part II. *Transactions of the Royal Society of Edinburgh* 32 (1884), 318–334.
- Alain C. Vaucher and Markus Reiher. 2018. Minimum Energy Paths and Transition States by Curve Optimization. *Journal of Chemical Theory and Computation* 14, 6 (2018), 3091–3099. <https://doi.org/10.1021/acs.jctc.8b00169>
- Bolun Wang, Zachary Ferguson, Tesseo Schneider, Xin Jiang, Marco Attene, and Daniele Panozzo. 2021. A Large-scale Benchmark and an Inclusion-based Algorithm for Continuous Collision Detection. *ACM Trans. Graph.* 40, 5 (2021), 1–16. <https://doi.org/10.1145/3460775>
- Wolfgang Wenzel and Kay Hamacher. 1999. Stochastic tunneling approach for global minimization of complex potential energy landscapes. *Physical Review Letters* 82, 15 (1999), 3003.
- Chris Yu, Henrik Schumacher, and Keenan Crane. 2021. Repulsive Curves. *ACM Trans. Graph.* 40, 2 (2021), 1–21. <https://doi.org/10.1145/3439429>
- Michalewicz Zbigniew. 1996. Genetic algorithms + data structures = evolution programs. In *Computational Statistics*. Springer-Verlag, 372–373. <https://doi.org/10.1007/978-3-662-03315-9>
- Ran Zhang, Thomas Auzinger, and Bernd Bickel. 2021. Computational Design of Planar Multistable Compliant Structures. *ACM Trans. Graph.* 40, 5 (2021), 1–16. <https://doi.org/10.1145/3453477>

## A DOWKER-THISTLETHWAITE NOTATION

The Dowker-Thistlethwaite (DT) notation uses a sequence of integers to encode the topological structure of a knot type. A *DT sequence*, or *code*, can be derived from a knot diagram with  $c$  crossings as a sequence of signed integers whose absolute value is an even number from 2 to  $2c$ . Given a knot diagram, the DT code can be computed by picking an arbitrary starting point and direction, and then label crossings in order of traversal. A negative sign is used to indicate that the strand with even label passes over at the crossing. The DT code is obtained by sorting the signed integers according to the associated odd labels  $1, 3, \dots, 2c - 1$ . A diagram of knot  $8_{21}$  and the corresponding DT code can be seen in the inset. Given a DT code, a 2D projection of the corresponding knot type can be reconstructed up to reflections. For detailed examples of DT code computation and knot reconstruction from DT code we refer to [Adams 2004]. A reconstructed knot diagram can be embedded in 3D as discussed e.g. in [Scharein 1998].



DT Code:  
[4, 8, -12, 2, 14, -6, 16, 10]

## B BRIDGE AND BRAID INDEX

Given a knot diagram, a bridge is a subarc that includes only over-crossings. The bridge number of the knot diagram is the least number of disjoint bridges that contain all over-crossings. The *bridge*

*index* of a knot type  $K$  is the minimum bridge number across all knot diagrams of type  $K$ . Equivalently, the bridge index can be defined as the minimal number of local maxima along a given direction across all the knot embeddings of type  $K$  [Adams 2004].

A braid can be imagined as a set of intertwined strands heading from left to right (see Figure 13). Alexander’s theorem [1923] guarantees that every knot is topologically equivalent to infinitely many closed braids. The *braid index* of a knot type  $K$  is the minimal number of strands needed to generate a closed braid of type  $K$ . Note that  $\text{bridge}(K) \leq \text{braid}(K)$ , as every braid can be arranged so that each of its strands contributes to the definition of the bridge index with a single local maximum.

## C LINK, TWIST, AND WRITHE OF A FRAMED CURVE

Given a smooth closed curve  $\mathbf{x}(s) \in \mathbb{R}^3$  parametrized by arc-length  $s \in [0, L_x]$ , and a family of framing vectors  $\mathbf{d}_1(s) \in \mathbb{R}^3$  such that  $\mathbf{d}_1(s) \perp \mathbf{x}'(s) \forall s$ , the *linking number*  $Lk$  of the framed curve  $(\mathbf{x}, \mathbf{d}_1)$  is defined by the Gauss double integral

$$Lk(\mathbf{x}, \mathbf{d}_1) = \frac{1}{4\pi} \int_0^{L_x} \int_0^{L_x} \frac{(\mathbf{x}(s) - \mathbf{y}(t)) \cdot (\mathbf{x}'(s) \times \mathbf{y}'(t))}{\|\mathbf{x}(s) - \mathbf{y}(t)\|^3} dt ds, \quad (2)$$

where  $\mathbf{y} = \mathbf{x} + \epsilon \mathbf{d}_1$  is an offset curve generated by displacing  $\mathbf{x}$  in the direction of  $\mathbf{d}_1$ , and  $\epsilon > 0$  is chosen small enough to guarantee that  $\mathbf{x}$  and  $\mathbf{y}$  do not intersect.

For a closed framed curve  $(\mathbf{x}, \mathbf{d}_1)$ , Călugăreanu’s theorem [1961] states that  $\text{link}(Lk)$  can be decomposed into the sum of *twist* ( $Tw$ ) and *writhe* ( $Wr$ )

$$Lk(\mathbf{x}, \mathbf{d}_1) = Tw(\mathbf{x}, \mathbf{d}_1) + Wr(\mathbf{x}), \quad (3)$$

where

$$Tw(\mathbf{x}, \mathbf{d}_1) = \frac{1}{2\pi} \int_0^{L_x} \mathbf{d}_1'(s) \cdot (\mathbf{x}'(s) \times \mathbf{d}_1(s)) ds, \quad (4)$$

and

$$Wr(\mathbf{x}) = \frac{1}{4\pi} \int_0^{L_x} \int_0^{L_x} \frac{(\mathbf{x}(s) - \mathbf{x}(t)) \cdot (\mathbf{x}'(s) \times \mathbf{x}'(t))}{\|\mathbf{x}(s) - \mathbf{x}(t)\|^3} dt ds. \quad (5)$$

Note that  $Wr(\mathbf{x})$  only depends on the curve but not on the framing  $\mathbf{d}_1$ . For more details on the geometric interpretation of these quantities see e.g. [O’Reilly 2017, Ch. 3].

A discrete version of eq. (3) has been applied to polygonal curves in the context of DNA modeling [Klenin and Langowski 2000]. For a discrete rod  $R = \{(\mathbf{x}_i, \mathbf{d}_1^i)\}_{i=0}^{n-1}$ , where  $\mathbf{x}_i$  are the nodal positions, and  $\mathbf{d}_1^i$  represent the first director of the adapted material frames orthogonal to edge  $i$ , the twist can be defined as

$$Tw(R) = \frac{1}{2\pi} \sum_{i=1}^n (\theta^i - \theta^{i-1} + \underline{m}_i) = \frac{1}{2\pi} \left( \Theta + \sum_{i=1}^n \underline{m}_i \right). \quad (6)$$

Here  $\underline{m}_i$  is the twist of the reference frame at node  $i$ , see [Bergou et al. 2010]. Note that cyclic indexing modulo  $n$  is implied for a closed periodic rod. The writhe of  $R$  can be computed from eq. (5), where the double integral reduces to a double sum over the set of all edge pairs, and the contribution of each pair can be evaluated exactly [Swigon et al. 1998]. The link of  $R$  is then given by the sum of its twist and writhe.